Interplay between intervalley scattering and impact ionization induced by intense terahertz pulses in InSb thin films

C. M. Garcia-Rosas,[1] X. Ropagnol,[1,2] L. Guiramand,[2] F. Blanchard,[2] and T. Ozaki[1,*]

[1] *Institut National de la Recherche Scientifique–Énergie Matériaux Télécommunications, 1650 Boulevard Lionel Boulet, Varennes, Québec, Canada J3X 1P7*

[2] *Département de Génie Électrique, École de Technologie Supérieure (ÉTS), 1100 Rue Notre-Dame Ouest, Montréal, Québec, Canada H3C 1K3*

(Received 23 March 2023; revised 14 December 2023; accepted 18 December 2023; published 8 January 2024)

In this paper, we reveal the intricate interplay between two major nonlinear terahertz (THz) effects: intervalley scattering and impact ionization, generated by an intense few-cycle THz pulse in an undoped (100) indium antimonide semiconductor at room temperature. Our results show an initial transmission enhancement when increasing the peak electric field up to 91 kV/cm, followed by increased absorption for higher fields. Our analytical model explains that the THz strength of 91 kV/cm, is the critical field where the bleaching of absorption (induced by intervalley scattering of electrons in the conduction band) is dominant below this field, whereas above it impact ionization starts to be the dominant energy loss mechanism. The temporal and amplitude change of the total average effective carrier mass and the total carrier density allow us to monitor the THz strength fields where each scattering effect plays a dominant role. We find that the change in the carrier populations is not the only factor that influences the current density, but indeed the average drift velocity of each valley is also a decisive factor, which is derived from the carrier momentum change. The developed theoretical model match very well qualitatively and quantitatively with the experimental results.

DOI: 10.1103/PhysRevB.109.045406

I. INTRODUCTION

Semiconductor thin films are the building blocks of modern industry, benefiting a wide range of technologies such as solar cells, power electronic devices, transistors, and sensors [1]. In a context where electromagnetic waves of terahertz (THz) frequencies will increasingly become an indispensable tool in our daily lives [2], it is clear that the ultrafast properties of semiconductor thin films are vital to manipulating and controlling these waves [3]. THz time-domain spectroscopy (THz-TDS) has proved to be a powerful tool in unraveling the ultrafast electronic properties of semiconductors [4–7]. More recently, with the advent of intense THz sources [8–10], the study of various nonlinear THz phenomena is providing access to new knowledge of materials that were out of reach using linear techniques [11–20]. As a result, nonlinear THz spectroscopy is opening new horizons in material science and the development of future ultrafast devices. For example, several studies of various phenomena such as effective mass anisotropy [11], intravalley and intervalley scattering [12–15], and high-order harmonic generation (HHG) [16,17] have been investigated in bulk, thin-film, and monolayer graphene, respectively. In addition, impact ionization, which can significantly affect the behavior and performance of semiconductor devices, is another nonlinear effect that has been studied extensively, but mainly in bulk and low-temperature samples [21–31].

Among the interesting candidates, indium antimonide (InSb) is a narrow band gap semiconductor with a large electron mobility of 7.7×10^4 cm^2 V^{-1} s^{-1} [32] and has the capability to work under extremely wide temperature conditions ranging from -270 to 300 °C [33]. InSb is also an intriguing test bed for nonlinear THz effects, especially to study the balance between different nonlinear mechanisms. In particular, the impact ionization process in InSb has been the subject of numerous theoretical and experimental studies [21–28,34–37]. Ganichev *et al.* experimentally showed for the first time highly nonlinear far-infrared absorption in *n*- and *p*-type InSb bulk wafers, creating a large number of free carriers due to the highly effective carrier multiplication triggered by impact ionization [21,22]. Further, carrier generation by impact ionization has been reported when an intense single-cycle THz pulse with a duration of $\leqslant$1 ps is transmitted through an *n*-type InSb wafer at 80 K [24–27]. Ašmontas and co-workers implemented a Monte Carlo simulation method and demonstrated that for THz electric fields higher than 8.5 kV/cm at 80 K, the impact ionization process in InSb starts to become the prominent nonlinear THz effect [23–25]. Using a two-dimensional nonlinear THz-TDS system in reflection configuration and at room temperature, Biasco *et al.* observed highly nonlinear effects in nominally undoped bulk InSb samples [34]. However, in these previous works, the authors mainly focused on carrier generation by impact ionization. This is because one would anticipate that impact ionization would be the dominant effect beyond among all nonlinear THz phenomena since the band gap of InSb (0.17 eV) is considerably smaller than the energy difference (0.51 eV) between the bottom of

*To whom all correspondence should be addressed: Tsuneyuki.Ozaki@inrs.ca

 ©2024 American Physical Society

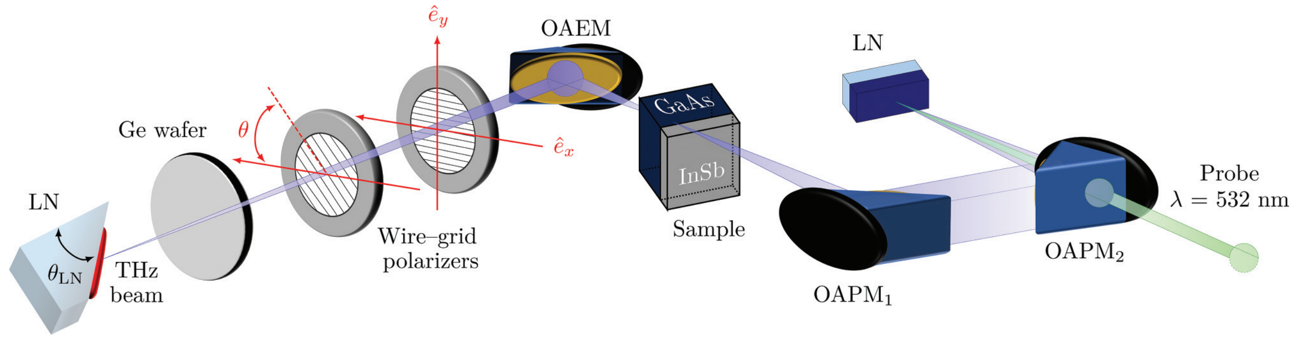

FIG. 1. Schematic experimental setup of the emitted THz radiation using an LN crystal and transmitted through two wire-grid polarizers, collected by an OAEM, and focused onto an InSb/GaAs sample.

the conduction band (Γ point) and the nearest satellite valley (*L* point).

In this paper, we show that this is, in fact, not the case. We find that despite the relatively significant energy difference between the Γ and *L* valleys, that intervalley scattering is the dominant effect at lower THz fields below 91 kV/cm. Subsequently, the impact ionization rate increases rapidly as the THz field is further increased, and eventually impact ionization becomes the dominant effect at higher fields above 100 kV/cm. To demonstrate this, we performed, at room temperature, nonlinear THz-TDS studies of an undoped thin film of InSb deposited on a gallium arsenide (GaAs) substrate using intense few-cycle THz pulses with incident peak electric fields ranging from 33 to 151 kV/cm. We experimentally observe a transmission enhancement for THz fields lower than 91 kV/cm, followed by a drop in transmission for higher intensity. To deepen our understanding of the nonlinear THz phenomenon that we experimentally observe, we develop a model that considers time-resolved carrier dynamics and impact ionization to explain the interaction of an InSb thin-film layer pumped by an intense few-cycle THz pulse. Our analytical model also reveals a critical THz field of 91 kV/cm. Electron intervalley scattering is the dominant mechanism for THz fields lower than 91 kV/cm. In contrast, for higher fields, the probability of impact ionization rapidly increases, starting to play a dominant role when the energy of the generated hot electrons is larger than the threshold energy $\varepsilon_{\rm th}$. In fact, the additional generation of electron-hole pairs due to impact ionization results in extra carrier generation in the Γ valley. Nevertheless, we also find that the change in the carrier populations is not the only factor that influences the current density, but indeed the average drift velocity of each valley is also a decisive factor, which is derived from the carrier momentum change. Our numerical simulations provide insight into the underlying fundamental mechanisms of the experimentally observed trends. The key to nonlinear THz field transmission in InSb is the intricate balance between intervalley scattering and impact ionization to the driving THz fields, leading to a nonlinear current density modulated by a nonlinear time-dependent conductivity.

II. EXPERIMENTAL SETUP

The experimental setup used to perform our THz measurements is the same as the one reported in Ref. [9]. In this setup, intense THz pulses are generated by optical rectification using the pulse front-tilt technique with a lithium-niobate (LN) crystal with a cut angle of 63°. The tilt of the wave front has been realized using an echelon mirror. The emitted THz radiation is collected by an off-axis ellipsoidal mirror (OAEM) placed 84 mm from the LN crystal. Then, the OAEM focuses the THz beam onto an InSb/GaAs sample or a GaAs bare substrate placed 33 mm from the OAEM. Between the LN crystal and the OAEM, we placed a germanium (Ge) wafer to block the residual leakage of the pump beam and its second harmonic generated by the LN crystal. Then, a pair of wire-grid polarizers were placed between the Ge wafer and the OAEM. The THz peak electric field was controlled by rotating the angle θ of the first wire-grid polarizer, while the second polarizer was fixed to ensure a perpendicular polarization of the THz pulse (see Fig. 1). The InSb sample under study, from MTI Corporation, is an undoped (100) InSb semiconductor thin-film layer with a carrier concentration of approximately 10^{17} cm^{-3} at room temperature. The thickness of the thin-film InSb layer is 500 nm, and the semi-insulating GaAs substrate is 0.5 mm thick with a resistivity higher than 10^8 $(\Omega\,\text{cm})^{-1}$. Ultimately, the THz radiation transmitted through the sample is collected by a first off-axis parabolic mirror (OAPM) and then focused by second OAPM on an electro-optical sensor (LN thin crystal).

III. EXPERIMENTAL RESULTS

The maximum incident THz peak electric field measured was 151 kV/cm at $\theta = 0°$, whereas in turn, the minimum THz peak electric field reached in this experiment was 33 kV/cm for $\theta = 62°$. Here, the incident THz peak field was directly measured by the modulation of the balanced photodiodes from the Pockel effect inside the electro-optic sensor [9,38]. Figure 2(a) shows the THz waveforms of the transmitted THz pulses through the GaAs substrate ($E_{\rm ref.}$) and the undoped InSb thin film ($E_{\rm trans.}$). Moreover, for frequencies above 1.6 THz, we start to observe a continuous high-frequency generation over the maximum transmission for THz peak electric fields between 77 and 105 kV/cm [see Fig. 2(b) and Sec. 1 of the Supplemental Material (SM) [39]]. Here, the high-frequency band generation is due to the rapid drop that the current density experiences [13].

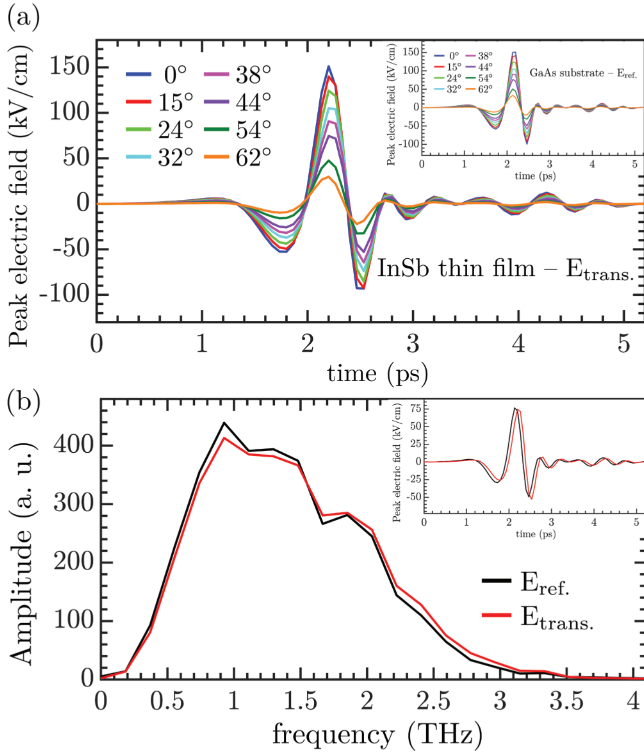

FIG. 2. (a) THz waveforms of the transmitted THz pulses through the GaAs substrate (inset) and the undoped InSb thin film deposited on a GaAs substrate. (b) Amplitude spectra of the transmitted THz pulse through the GaAs substrate (solid black lines) and the InSb/GaAs sample (solid red lines), with a THz peak electric field of 77 kV/cm. Inset: Corresponding THz waveforms.

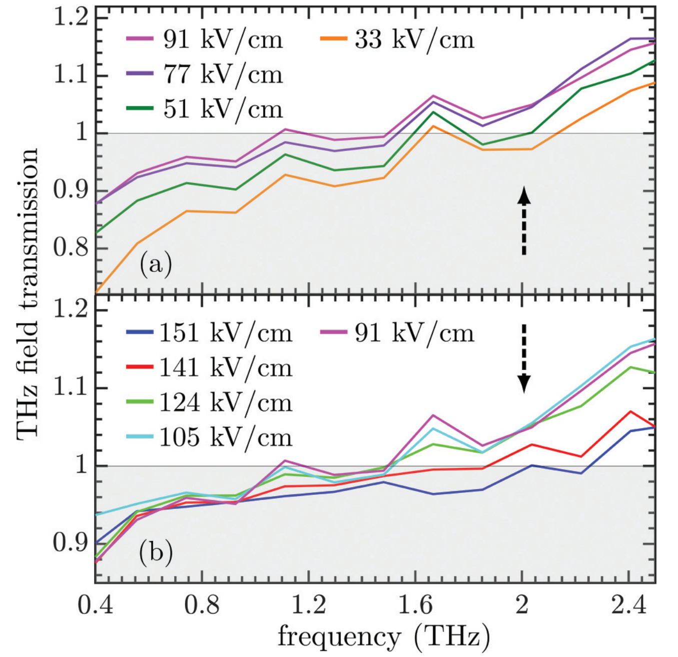

FIG. 3. Normalized THz field transmission at different THz field strengths as a function of the frequency for THz peak electric fields (a) lower and (b) higher than 91 kV/cm. The upwards and downwards black dashed arrows depict the increasing and decreasing trend of the transmission, respectively.

Figure 3 illustrates the normalized spectrally resolved THz field transmission T, where [40]

$$T = \frac{|E_{\text{trans.}}(\omega)e^{i\phi_{\text{trans.}}(\omega)}|}{|E_{\text{ref.}}(\omega)e^{i\phi_{\text{ref.}}(\omega)}|}. \tag{1}$$

Here, $E_{\text{ref.}}(\omega)$ and $E_{\text{trans.}}(\omega)$ are the spectral amplitudes, and $\phi_{\text{ref.}}(\omega)$ and $\phi_{\text{trans.}}(\omega)$ are the spectral phases of the corresponding reference and transmitted THz pulses, respectively, as a function of the frequency. In Fig. 3(a), we observe a nonlinear transmission enhancement for the THz field is ranging from 33 up to 91 kV/cm, with an average increase of 11%. On average, the normalized transmission is smaller than 1 for frequencies below 2.15 THz and greater than 1 for higher frequencies. However, as the field strength is increased, the normalized transmission is enhanced and the frequency threshold where the normalized transmission is higher than 1 start to decrease. For example, at 33 kV/cm, the frequency threshold is at 2.15 THz, whereas for 91 kV/cm it is at 1.55 THz. Nonlinear transmission enhancement is caused by the carriers that have been accelerated by the driven THz field and scattered to higher satellite valleys (i.e., the L valley), where the carrier effective mass is higher. As a result, the carrier's mobility will be reduced, decreasing the overall macroscopic terahertz conductivity of the thin film. These observations are in good agreement with previously published data [13]. More surprisingly, by continuing to increase the THz peak electric field, we observe a nonlinear decrease in the normalized transmission while we keep increasing the THz field from 91 up to 151 kV/cm [see Fig. 3(b)]. Between 91, 105, and 124 kV/cm, the normalized transmission decrease is nonuniform. However, we start to observe a clear tendency of a drop in transmission for frequencies higher than 1.6 THz.

We ascribe this response to the impact ionization process driven by high-field THz pulses [26,34,37], where the energy of the carriers is greater that ε_{th} and an electron is scattered from the valence band to the conduction band. For 141 and 151 kV/cm, there is a drastic drop in transmission even for frequencies below 1 THz. By comparing the temporal profiles of the total average effective carrier mass and the total carrier density, we observe that intervalley scattering plays a dominant role earlier in time and with a higher amplitude than impact ionization at low THz fields. On the other hand, for higher-field THz pulses, the intervalley scattering is still induced earlier in time but with less intensity than impact ionization, becoming the dominant energy loss mechanism (see Sec. 6 of the SM [39]). This interplay between intervalley scattering and impact ionization leads to highly nonlinear THz conductivity at low and high frequencies, and hence to the transmission (see Sec. 4 of the SM [39]). However, the relatively modest change in the transmission is a direct consequence of working with an undoped thin film, where the carrier concentration is only 10^{17} cm^{-3} [41]. Nevertheless, it is important to noticed that a stronger impact ionization probability has been observed in InSb [23–27] and in other semiconductor crystals such as Si and InAs [25,30,31], but such semiconductors were pumped by either an extremely high THz field strength of several MV/cm or at a cryogenic temperature.

To explain the strong nonlinear transmission observed at low and high fields, in our model, we used a system of differential rate equations incorporating the Keldysh impact ionization model [26,29–31,42] and the intravalley and intervalley scattering mechanisms [12,13,15,43] (see Sec. 2 of the SM for details [39]). Additionally, we considered an initial carrier concentration of the InSb thin film equal to 10^{17} cm^{-3}. By fitting the experimental data, the energy relaxation time remains constant at 5 ps for carriers in both the Γ and *L* valley. The energy relaxation time rate is similar to that already reported in Refs. [26,34]. Additionally, as previously discussed by other authors [23–26,34], since the energy separation between the *X* valley and the top of the valence band is six times the value of the band gap, in our model, we do not study the carrier dynamics in the *X* valley for InSb, and we only consider the energy transfer between the carriers in the Γ and *L* valleys.

The intricate balance between intervalley scattering and impact ionization in THz-driven InSb results in a highly nonlinear change in the carrier population of the Γ and *L* valleys. We find that the change in the carrier populations is not the only factor that influences the current density, but indeed the average drift velocity of each valley is also a decisive factor, which is derived from the carrier momentum change, as illustrated in the calculations shown in Fig. 4. At low THz peak electric fields, the carriers remain in the Γ valley and basically follow the incident THz temporal profile [12,13,15,43]. Our numerical calculations show that as we increase the applied THz field to 91 kV/cm, we observe intervalley transitions from the Γ valley to the *L* valley (see Fig. S2 of the SM [39]). Here, once the ponderomotive acceleration is strong enough, the carriers acquire sufficient kinetic energy to efficiently undergo intervalley scattering from the Γ to the *L* valley. On the other hand, for THz field strengths above 91 kV/cm, the intense THz transients keep accelerating the remaining carriers. Figures 4(c) and 4(d) show a drastic change in the carrier population in the Γ and *L* valley, resulting in a temporal contrast of the current density [13,15]. More interestingly, at these high fields, the electrons start to acquire sufficient energy to induce impact ionization, where a THz-accelerated electron in the conduction band scatters an electron from the valence band to the conduction band. This creates an additional *e*-*h* pair [8], resulting in additional carrier generation in the Γ valley. Therefore, in Figs. 4(c) and 4(d), we attribute the smooth increase in the carrier population in the Γ valley to the impact ionization process, which starts to become the dominant energy loss mechanism when the hot electrons have energy larger than $\varepsilon_{\text{th}}^{\Gamma} = 0.17$ eV.

Next, we compute the average transmission over the entire spectrum by calculating the power transmission of the entire THz pulse, also known as the integrated transmission, where [40]

$$\langle T \rangle = \frac{\int_{-\infty}^{\infty} E_{\text{trans.}}^2(t)dt}{\int_{-\infty}^{\infty} E_{\text{ref.}}^2(t)dt}. \tag{2}$$

Figure 5 shows the calculated power transmission of the entire THz pulse as a function of the peak electric field for experimental and simulated data. There is a qualitative and quantitative agreement between the experimental and

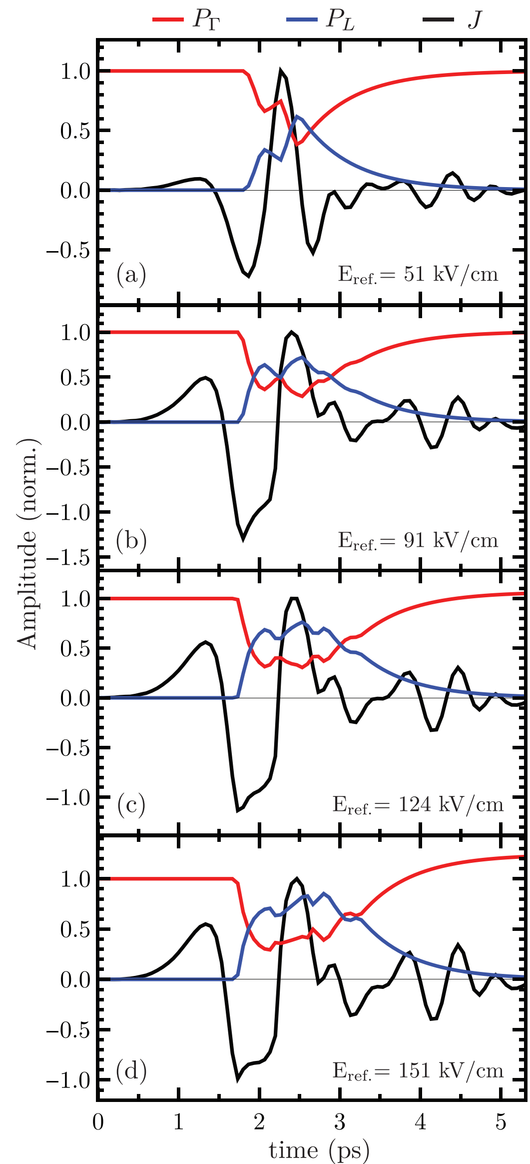

FIG. 4. Normalized temporal current density (solid black lines), and carrier populations in the Γ (solid red lines) and *L* (solid blue lines) valleys as a function of time for different peak electric fields, with the initial carrier concentration of $n_0(t = 0) = 1\times10^{17}$ cm^{-3} at room temperature.

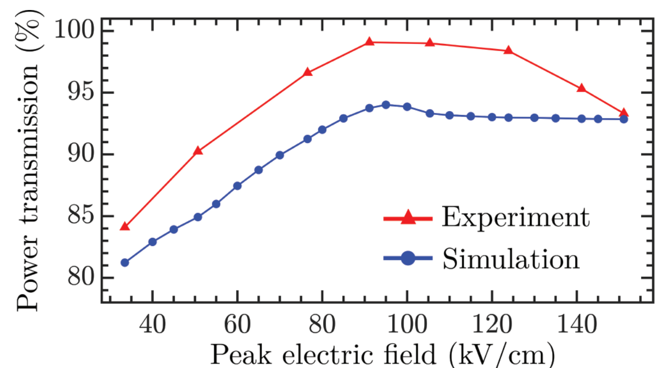

FIG. 5. Experimental and simulated power transmission coefficient as a function of the peak field of the THz pulse.

simulated power transmission curves. Our temporal carrier dynamics and impact ionization model is in good agreement with the observed trends, showing that the threshold electric field of impact ionization is ≈91 kV/cm, which is the same value obtained in our experiments. However, the quantitative discrepancies are due to the simple system of differential rate equations that only describe the momentum and energy losses of the excited charge carriers during impact ionization. Moreover, experimentally observed power transmission for 33 kV/cm is 84% and reaches a maximum of 99% at ≈91 kV/cm. The increase of ≈15% in power transmission agrees with the calculated THz peak field transmission values shown in Fig. 3(a). On the other hand, for peak electric fields higher than ≈91 kV/cm, the power transmission shows an ≈5% decrease, in agreement with plots of the THz field transmission [see Fig. 3(b)].

IV. SUMMARY

We study the nonlinear transmission of intense THz pulses through an undoped InSb semiconductor thin film at room temperature. We observe transmission enhancement when increasing the peak field up to 91 kV/cm, followed by increased absorption for higher fields. We attribute the transmission enhancement to absorption bleaching induced by intervalley scattering of electrons in the conduction band, and the increased absorption to impact ionization within the InSb sample, even though the sample is undoped [26,34]. Our model explains these observations and confirms the presence of an intricate balance between intervalley scattering and impact ionization, where for a peak electric field higher than 91 kV/cm, the hot electrons start to gain energy larger than $\varepsilon_{th}^{\Gamma}$ and induce impact ionization. Our numerical results show a highly nonlinear change in the carrier population of the Γ and L valleys due to the interplay of these two scattering processes. Finally, the spectra of the THz field transmissions show a nonlinear transmission increase of ≈15% and the decrease is estimated to be ≈5%.

ACKNOWLEDGMENTS

This work is supported by the Natural Sciences and Engineering Research Council of Canada (NSERC) Grant No. RGPIN-2019-06811. C.M.G.R. gratefully acknowledges financial support from Fonds de Recherche du Quebec - Nature et Technologies (FRQNT) and the PBEEE V1 scholarship (319758). F.B. gratefully acknowledges financial support from NSERC (2016-05020) and the Canada Research Chair (CRC-2019-127). We thank X. Chai for the insightful recommendation on testing an undoped (100) InSb thin-film sample.

[1] O. Sancakoglu, Technological background and properties of thin film semiconductors, in *21st Century Surface Science: A Handbook*, edited by P. Pham, P. Goel, S. Kumar, and K. Yadav (IntechOpen, London, 2020), pp. 49–59.

[2] A. Leitenstorfer, A. S. Moskalenko, T. Kampfrath, J. Kono, E. Castro-Camus, K. Peng, N. Qureshi, D. Turchinovich, K. Tanaka, A. Markelz *et al.*, J. Phys. D: Appl. Phys. **56**, 223001 (2023).

[3] H. Hafez, X. Chai, A. Ibrahim, S. Mondal, D. Férachou, X. Ropagnol, and T. Ozaki, J. Opt. **18**, 093004 (2016).

[4] M. Tonouchi, Nat. Photon. **1**, 97 (2007).

[5] M. C. Nuss and J. Orenstein, Terahertz time-domain spectroscopy (THz-TDS), in *Millimeter-Wave Spectroscopy of Solids*, edited by G. Gruener, Topics in Applied Physics Vol. 74 (Springer, Berlin, 1997), pp. 7–50.

[6] J. Neu and C. A. Schmuttenmaer, J. Appl. Phys. **124**, 231101 (2018).

[7] L. Duvillaret, F. Garet, and J.-L. Coutaz, IEEE J. Sel. Top. Quantum Electron. **2**, 739 (1996).

[8] H. Hirori, K. Shinokita, M. Shirai, S. Tani, Y. Kadoya, and K. Tanaka, Nat. Commun. **2**, 594 (2011).

[9] L. Guiramand, J. E. Nkeck, X. Ropagnol, T. Ozaki, and F. Blanchard, Photon. Res. **10**, 340 (2022).

[10] B. Green, S. Kovalev, V. Asgekar, G. Geloni, U. Lehnert, T. Golz, M. Kuntzsch, C. Bauer, J. Hauser, J. Voigtlaender *et al.*, Sci. Rep. **6**, 22256 (2016).

[11] F. Blanchard, D. Golde, F. H. Su, L. Razzari, G. Sharma, R. Morandotti, T. Ozaki, M. Reid, M. Kira, S. W. Koch, and F. A. Hegmann, Phys. Rev. Lett. **107**, 107401 (2011).

[12] L. Razzari, F. H. Su, G. Sharma, F. Blanchard, A. Ayesheshim, H.-C. Bandulet, R. Morandotti, J.-C. Kieffer, T. Ozaki, M. Reid, and F. A. Hegmann, Phys. Rev. B **79**, 193204 (2009).

[13] X. Chai, X. Ropagnol, S. M. Raeis-Zadeh, M. Reid, S. Safavi-Naeini, and T. Ozaki, Phys. Rev. Lett. **121**, 143901 (2018).

[14] F. Blanchard, X. Chai, T. Tanaka, T. Arikawa, T. Ozaki, R. Morandotti, and K. Tanaka, Opt. Lett. **43**, 4997 (2018).

[15] C. M. Garcia-Rosas, X. Chai, X. Ropagnol, and T. Ozaki, Phys. Rev. B **104**, L161201 (2021).

[16] H. A. Hafez, S. Kovalev, J. C. Deinert, Z. Mics, B. Green, N. Awari, M. Chen, S. Germanskiy, U. Lehnert, J. Teichert, Z. Wang, K. J. Tielrooij, Z. Liu, Z. Chen, A. Naritaa, K. Müllen, M. Bonn, M. Gensch, and D. Turchinovich, Nature (London) **561**, 507 (2018).

[17] H. A. Hafez, S. Kovalev, K.-J. Tielrooij, M. Bonn, M. Gensch, and D. Turchinovich, Adv. Opt. Mater. **8**, 1900771 (2020).

[18] S. Kovalev, H. A. Hafez, K.-J. Tielrooij, J.-C. Deinert, I. Ilyakov, N. Awari, D. Alcaraz, K. Soundarapandian, D. Saleta, S. Germanskiy, M. Chen, M. Bawatna, B. Green, F. H. L. Koppens, M. Mittendorff, M. Bonn, M. Gensch, and D. Turchinovich, Sci. Adv. **7**, eabf9809 (2021).

[19] F. Langer, M. Hohenleutner, C. P. Schmid, C. Poellmann, P. Nagler, T. Korn, C. Schüller, M. S. Sherwin, U. Huttner, J. T. Steiner, S. W. Koch, M. Kira, and R. Huber, Nature (London) **533**, 225 (2016).

[20] F. Langer, C. P. Schmid, S. Schlauderer, J. F. M. Gmitra, P. Nagler, C. Schüller, T. Korn, P. G. Hawkins, J. T. Steiner, U. Huttner, S. W. Koch, M. Kira, and R. Huber, Nature (London) **557**, 76 (2018).

[21] S. D. Ganichev, A. P. Dmitriev, S. A. Emel'yanov, Y. V. Terent'ev, I. D. Yaroshetskii, and I. N. Yassievich, Zh. Eksp. Teor. Fiz. **90**, 445 (1986) [J. Exp. Theor. Phys. **63**, 256 (1986)].

[22] S. D. Ganichev, J. Diener, and W. Prettl, Appl. Phys. Lett. **64**, 1977 (1994).

[23] S. Ašmontas, R. Raguotis, and S. Bumelienė, Semicond. Sci. Technol. **28**, 025019 (2013).

[24] S. Ašmontas, R. Raguotis, and S. Bumelienė, Appl. Phys. A **120**, 1241 (2015).

[25] S. Ašmontas, S. Bumelienė, J. Gradauskas, R. Raguotis, and A. Sužiedėlis, Sci. Rep. **10**, 10580 (2020).

[26] M. C. Hoffmann, J. Hebling, H. Y. Hwang, K.-L. Yeh, and K. A. Nelson, Phys. Rev. B **79**, 161201(R) (2009).

[27] H. Wen, M. Wiczer, and A. M. Lindenberg, Phys. Rev. B **78**, 125203 (2008).

[28] T. Kobayashi, J. Appl. Phys. **48**, 3154 (1977).

[29] E. Cartier, M. Fischetti, E. Eklund, and F. McFeely, Appl. Phys. Lett. **62**, 3339 (1993).

[30] M. Bejide, Y. Li, N. Stavrias, B. Redlich, T. Tanaka, V. D. Lam, N. T. Tung, and E. Janssens, Opt. Express **29**, 170 (2021).

[31] A. V. Ovchinnikov, O. V. Chefonov, M. B. Agranat, A. V. Kudryavtsev, E. D. Mishina, and A. A. Yurkevich, Opt. Express **29**, 26093 (2021).

[32] Y. A. Goldberg, Indium antimonide (InSb), in *Handbook Series on Semiconductor Parameters*, edited by M. Levinshtein, S. Rumyantsev, and M. Shur (World Scientific, Singapore, 1996), Vol. 1, pp. 191–212.

[33] J. Jankowski, S. El-Ahmar, and M. Oszwaldowski, Sensors **11**, 876 (2011).

[34] S. Biasco, F. Burri, S. Houver, E. Abreu, M. Savoini, and S. L. Johnson, Phys. Rev. B **106**, 235201 (2022).

[35] J. T. Devreese, R. G. Van Welzenis, and R. P. Evrard, Appl. Phys. A **29**, 125 (1982).

[36] H. Tanimura, J. Kanasaki, and K. Tanimura, Sci. Rep. **4**, 6849 (2014).

[37] H. Tanimura, J. Kanasaki, and K. Tanimura, Phys. Rev. B **91**, 045201 (2015).

[38] F. Amirkhan, R. Sakata, K. Takiguchi, T. Arikawa, T. Ozaki, K. Tanaka, and F. Blanchard, J. Opt. Soc. Am. B **36**, 2593 (2019).

[39] See Supplemental Material at http://link.aps.org/supplemental/10.1103/PhysRevB.109.045406 for a discussion of high-frequency generation, the numerical simulation on carrier dynamics and impact ionization, including a description of the intervalley scattering, average carrier energy, and impact ionization process, and where we also determine the dielectric function and conductivity of InSb, and the average effective carrier mass and total carrier density, which includes Refs. [8,11–13,15,24–26,29–32,37,42–64].

[40] H. Y. Hwang, N. C. Brandt, H. Farhat, A. L. Hsu, J. Kong, and K. A. Nelson, J. Phys. Chem. B **117**, 15819 (2013).

[41] R. Ulbricht, E. Hendry, J. Shan, T. F. Heinz, and M. Bonn, Rev. Mod. Phys. **83**, 543 (2011).

[42] L. V. Keldysh, JETP **48**, 1692 (1965) [Sov. Phys. JETP **21**, 1135 (1965)].

[43] F. H. Su, F. Blanchard, G. Sharma, L. Razzari, A. Ayesheshim, T. L. Cocker, L. V. Titova, T. Ozaki, J.-C. Kieffer, R. Morandotti, M. Reid, and F. A. Hegmann, Opt. Express **17**, 9620 (2009).

[44] G. Sharma, L. Razzari, F. H. Su, F. Blanchard, A. Ayesheshim, T. L. Cocker, L. V. Titova, H. C. Bandulet, T. Ozaki, J. C. Kieffer, R. Morandotti, M. Reid, and F. A. Hegmann, IEEE Photon. J. **2**, 578 (2010).

[45] A. T. Tarekegne, K. Iwaszczuk, M. Zalkovskij, A. C. Strikwerda, and P. U. Jepsen, New J. Phys. **17**, 043002 (2015).

[46] S. T. Schaefer, S. Gao, P. T. Webster, R. R. Kosireddy, and S. R. Johnson, J. Appl. Phys. **127**, 165705 (2020).

[47] M. Lundstrom, *Fundamentals of Carrier Transport*, 2nd ed. (Cambridge University Press, Cambridge, UK, 2000).

[48] K. Reimann, Rep. Prog. Phys. **70**, 1597 (2007).

[49] W. Kuehn, P. Gaal, K. Reimann, M. Woerner, T. Elsaesser, and R. Hey, Phys. Rev. B **82**, 075204 (2010).

[50] W. Kuehn, P. Gaal, K. Reimann, M. Woerner, T. Elsaesser, and R. Hey, Phys. Rev. Lett. **104**, 146602 (2010).

[51] P. Bowlan, E. Martinez-Moreno, K. Reimann, T. Elsaesser, and M. Woerner, Phys. Rev. B **89**, 041408(R) (2014).

[52] S. M. Sze and K. K. Ng, *Physics of Semiconductor Devices*, 3rd ed. (Wiley, Hoboken, NJ, 2006).

[53] R. Boyd, *Nonlinear Optics* (Academic Press/Elsevier Science, Amsterdam, 2003).

[54] A. M. Anile and S. D. Hern, VLSI Des. **15**, 681 (2002).

[55] A. Dargys, R. Sedrakyan, and J. Pôela, J. Phys. Status Solidi **45**, 387 (1978).

[56] D. R. Larson, NASA STI/Recon Technical Report No. **83**, 10416 (1981).

[57] M. Alouani, L. Brey, and N. E. Christensen, Phys. Rev. B **37**, 1167 (1988).

[58] P. Jepsen, J. Infrared, Millimeter, Terahertz Waves **40**, 395 (2019).

[59] P. Van den Berg and J. Borburgh, Appl. Phys. **3**, 55 (1974).

[60] S. C. Howells and L. A. Schlie, Appl. Phys. Lett. **69**, 550 (1996).

[61] J. G. Rivas, C. Janke, P. H. Bolivar, and H. Kurz, Opt. Express **13**, 847 (2005).

[62] V. Giannini, A. Berrier, S. A. Maier, J. A. Sánchez-Gil, and J. G. Rivas, Opt. Express **18**, 2797 (2010).

[63] T. H. Isaac, J. Gómez Rivas, J. R. Sambles, W. L. Barnes, and E. Hendry, Phys. Rev. B **77**, 113411 (2008).

[64] A. P. Long, P. H. Beton, and M. J. Kelly, J. Appl. Phys. **62**, 1842 (1987).